



**HAL**  
open science

## Characterization of early ultrastructural changes in the cerebral white matter of CADASIL small vessel disease using high pressure freezing/freeze-substitution Authors

Rikesh Rajani, Nicolas Dupré, Valérie Domenga-denier, Guillaume van Niel, Xavier Heiligenstein, Anne Joutel

### ► To cite this version:

Rikesh Rajani, Nicolas Dupré, Valérie Domenga-denier, Guillaume van Niel, Xavier Heiligenstein, et al.. Characterization of early ultrastructural changes in the cerebral white matter of CADASIL small vessel disease using high pressure freezing/freeze-substitution Authors. *Neuropathology and Applied Neurobiology*, 2021, 47 (5), pp.694-704. 10.1111/nan.12697 . inserm-03632100

**HAL Id: inserm-03632100**

**<https://inserm.hal.science/inserm-03632100>**

Submitted on 6 Apr 2022

**HAL** is a multi-disciplinary open access archive for the deposit and dissemination of scientific research documents, whether they are published or not. The documents may come from teaching and research institutions in France or abroad, or from public or private research centers.

L'archive ouverte pluridisciplinaire **HAL**, est destinée au dépôt et à la diffusion de documents scientifiques de niveau recherche, publiés ou non, émanant des établissements d'enseignement et de recherche français ou étrangers, des laboratoires publics ou privés.

# **Characterization of early ultrastructural changes in the cerebral white matter of CADASIL small vessel disease using high pressure freezing/freeze-substitution**

## **Authors**

Rikesh M. Rajani <sup>1</sup>, Nicolas Dupré <sup>1</sup>, Valérie Domenga-Denier <sup>1</sup>, Guillaume Van Niel <sup>1,2</sup>, Xavier Heiligenstein <sup>3</sup>, Anne Joutel <sup>1,2,4</sup>

## **Affiliations**

- 1- Institute of Psychiatry and Neurosciences of Paris, Inserm U1266, Université de Paris, Paris, France.
- 2- GHU Paris Psychiatrie et Neurosciences, Hôpital Sainte Anne, Paris, France
- 3- CryoCapCell, Inserm U1195, Université Paris Sud, Le Kremlin-Bicêtre, France
- 4- Department of Pharmacology, College of Medicine, University of Vermont, Burlington, VT, USA

## **Corresponding author:**

Anne Joutel, Inserm U1266, Institute of Psychiatry and Neurosciences of Paris, 102-108 rue de la Santé, 75014 Paris, France

Email: [anne.joutel@inserm.fr](mailto:anne.joutel@inserm.fr). Tel: +33 1 40 78 92 96

**Short running title:** Early white matter changes in CADASIL

**Text word counts** (does not include title, abstract, references, table, legends): 4526

**Number of figures:** 7

**Supplementary material:** 3 figures, 1 table

**Keywords:** CADASIL, small vessel disease, white matter, high pressure freezing/freeze-substitution, myelin splitting, inner tongue

## **Abstract**

**Aims.** The objective of this study was to elucidate the early white matter changes in CADASIL small vessel disease.

**Methods.** We used high pressure freezing and freeze substitution (HPF/FS) in combination with high resolution electron microscopy (EM), immunohistochemistry and confocal microscopy of brain specimens from control and CADASIL (*TgNotch3<sup>R169C</sup>*) mice aged 4 to 15 months to study white matter lesions in the corpus callosum.

**Results.** We first optimized the HPF/FS protocol in which samples were chemically prefixed, frozen in a sample carrier filled with 20% polyvinylpyrrolidone and freeze-substituted in a cocktail of tannic acid, osmium tetroxide and uranyl acetate dissolved in acetone. EM analysis showed that CADASIL mice exhibit significant splitting of myelin layers and enlargement of the inner tongue of small calibre axons from the age of 6 months, then vesiculation of the inner tongue and myelin sheath thinning at 15 months of age. Immunohistochemistry revealed an increased number of oligodendrocyte precursor cells, although only in older mice, but no reduction in the number of mature oligodendrocytes at any age. The number of Iba1 positive microglial cells was increased in older but not in younger CADASIL mice, but the number of activated microglial cells (Iba1 and CD68 positive) was unchanged at any age.

**Conclusion.** We conclude that early WM lesions in CADASIL affect first and foremost the myelin sheath and the inner tongue, suggestive of a primary myelin injury. We propose that those defects are consistent with a hypoxic/ischaemic mechanism.

## **List of abbreviations**

CADASIL: Cerebral autosomal dominant angiopathy with subcortical infarcts and leukoencephalopathy

EM: electron microscopy

HPF/FS: high pressure freezing and freeze substitution

K-S: Karlsson-Schultz

MBP: myelin basic protein

OPC: oligodendrocyte precursor cell

PB: phosphate buffer

PVP: polyvinylpyrrolidone

SEM: standard error of the mean

SVD: small vessel disease

WM: white matter

WT: wild-type

## Introduction

Cerebral small vessel disease (SVD) is the leading cause of vascular cognitive impairment that typically manifests with lacunar infarcts and white matter (WM) lesions (1). Cerebral autosomal dominant angiopathy with subcortical infarcts and leukoencephalopathy (CADASIL) is the most common monogenic form of SVD, caused by highly stereotyped mutations in NOTCH3, a receptor which is predominantly expressed in pericytes and smooth muscle cells around small vessels. Unlike sporadic SVD, comorbidities and age-related pathologies are uncommon in CADASIL patients. Therefore, CADASIL is now widely recognized as an invaluable model for studying mechanisms of SVD (2).

One of the earliest and most consistent features of CADASIL observed on brain magnetic resonance imaging is the presence of WM hyperintensities. These present as punctiform lesions from 30 years of age, and become more diffuse and symmetrical with age (2). The volume of these WM hyperintensities is mainly related to deficits in executive functioning, and especially in the speed of cognitive processing, the earliest and most prominent cognitive manifestations of CADASIL and SVD in general (3,4). Several studies strongly suggest that histopathological correlates of WM changes in SVD are heterogeneous (5). Our recent analysis of post-mortem brain tissue from patients with CADASIL confirmed this. Staining of tissue sections with Luxol fast blue, Haematoxylin & Eosin or anti-fibrinogen antibody, used as a marker of blood brain barrier leakage, revealed that WM lesions encompass at least 3 distinct categories of damage, namely: (i) WM lesions around lacunes, characterized by WM pallor with strong anti-fibrinogen staining; (ii) WM lesions surrounding enlarged perivascular spaces characterized by a non-uniform disorganization and pallor of the WM, with marked anti-fibrinogen staining, that bear some similarity to lesions which have previously been described as microinfarcts; and (iii) a category which we termed pure WM lesions that exhibit myelin pallor, but do not contain any overt pathology and is essentially devoid of fibrinogen leakage (6). Because post-mortem tissue from CADASIL patients generally represents a late stage of the disease, the chronological order of these 3 categories of WM damage cannot be determined. The Tg*Notch3*<sup>R169C</sup> mouse, a well characterized model of CADASIL, exhibits WM changes initially in the form of increased punctate staining using a specific monoclonal antibody (SMI-94) against myelin basic protein (MBP) — which is thought to mark uncompacted or degraded myelin — and later in life (20 months) as a pallor and vacuolization of WM tracts using Luxol fast blue staining (7–9). Importantly, the Tg*Notch3*<sup>R169C</sup> mouse does not show any signs of lacunes or enlarged perivascular spaces, suggesting that pure WM lesions are the earliest WM changes in CADASIL (7).

The mechanism that leads to these pure WM lesions is still unknown. Experimental studies have bolstered the idea that WM lesions might be caused by an increase in blood brain barrier permeability as a result of pericyte deficiency (10). However, our recent work studying pericyte labelling, endogenous blood-borne proteins, and injected exogenous small or large tracers has shown

that pericyte coverage is unaltered and blood brain barrier integrity is preserved in the damaged WM of *TgNotch3*<sup>R169C</sup> mice, a finding consistent with the lack of fibrinogen leakage in pure WM lesions in tissue sections from patients (6). This suggests that in order to understand this important feature of CADASIL, it is necessary to study the WM directly at an early stage of the disease.

WM fibres are axons surrounded by a myelin sheath, a multi-layered stack of self-associating plasma membranes tightly wrapped around the axon. Electron microscopy (EM) provides the necessary and required resolution to study WM fibres. However, in samples fixed and dehydrated using conventional methods, at 4°C or room temperature, preservation of myelin is a notorious problem, since the multilamellar structure tends to split upon chemical fixation or dehydration. While optimization of this technique can lead to excellent preservation in younger animals, this becomes particularly deleterious in older animals or those with severe WM damage. High pressure freezing (HPF), with or without prior chemical fixation, in combination with freeze substitution (FS) has recently emerged as a valuable alternative to the standard preparation of EM samples. This technique involves freezing the sample rapidly at a high pressure (2100 bar) to transform water into an amorphous state, preventing the formation of ice crystals, and then carrying out the dehydration step at temperatures below freezing over several days to hold the tissue structure in place and reduce artefacts (11,12).

In this study, we assessed WM changes at an early stage of CADASIL, at both the ultrastructural and cellular levels. To achieve this, we used the *TgNotch3*<sup>R169C</sup> mouse model, and because WM changes in this model develop with an anteroposterior and medio-lateral gradient (6), we selected the medial part of the genu of the corpus callosum. To study the WM at the ultrastructural level, we optimized a novel protocol including chemical fixation of the samples followed by HPF/FS in a cocktail of tannic acid, osmium tetroxide and uranyl acetate dissolved in acetone. To further analyse the WM at the cellular level, we used immunohistochemistry in combination with confocal microscopy. Results presented in this study provide insight into the earliest substrates of WM changes in CADASIL that suggest a primary myelin defect in this disease, and help to understand the mechanisms of this defect.

## **Methods**

### Animals

*TgNotch3*<sup>R169C</sup> mice overexpress the rat *Notch3* gene containing the mutation R169C found in CADASIL patients and were maintained on an FVB/N background (7). As controls, we used *TgNotch3*<sup>WT</sup> mice, overexpressing the wild type rat *Notch3* gene, and wild type mice interchangeably, as it has previously been shown that there are no white matter differences between *TgNotch3*<sup>WT</sup> mice and wild type mice (7,8). One 15-month-old wild type mouse and one 15-month-old *TgNotch3*<sup>R169C</sup> mouse was male; the rest of the animals used in this study were female.

### Ethics approval

Animal (mouse) experiments were approved by our local institutional Animal Care and Use Committees (CEEA9 and CEEA34, registration numbers 95 and 19-031) and by the French government (Ministère de l'Enseignement Supérieur et de la Recherche, authorizations #03653.02 and APAFiS #21100-2019041816189580v4).

### Preparation of tissue samples for EM analysis

Mice were deeply anaesthetized with sodium pentobarbital (80 mg/kg) and transcardially perfused with 0.1M heparinized phosphate buffer (PB) followed by Karlsson-Schultz fixative (K-S fix; 4% paraformaldehyde (PFA), 2.5% glutaraldehyde in 0.1M PB). Brains were extracted, split into hemispheres, and fixed overnight in K-S fix at 4°C. For processing using HPF/FS, 100µm thick sagittal sections were cut using a Leica VT1200S vibratome. For processing using conventional techniques, samples were further fixed for 1 week in 1% PFA in PB, before 1 mm thick sagittal sections were cut using a brain matrix. From these sections, a 2 mm diameter disc containing the most anterior portion of the corpus callosum (genu) at the midline was punched out of the section using a biopsy punch.

### Processing using HPF/FS

Prefixed samples were immediately transported to the HPF machine in a solution of 1% PFA in PB on ice. Specimens were placed in 3 mm diameter aluminium sample carriers within a solution of 20% polyvinylpyrrolidone (PVP; MW=10,000) in PB, and frozen using a HPM Live µ high pressure freezing machine (CryoCapCell, France). Samples were stored for up to 1 week in liquid nitrogen before freeze substitution. Freeze substitution was carried out using a Leica EM AFS machine by modifying a previously used protocol (13). Briefly, samples were incubated in 0.1% tannic acid in acetone for 24h at -90°C followed by 4 acetone washes each of 30mins at -90°C. Samples were then incubated in 2% osmium tetroxide, 0.1% uranyl acetate in acetone for 32-56h at -90°C, before the temperature was raised at 5°C/h to -20°C, then incubated for 16h at -20°C, followed by a temperature rise of 10°C/h to 4°C, followed by a 1h incubation at 4°C. Samples were then washed in acetone (4x 30 minutes at 4°C, followed by 1 hour while temperature was raised to room temperature), before being incubated in increasing concentrations of Epon in acetone (33% for 2h, 50% for 2h, 67% for 2h, 90% overnight, 100% for 2h, 100% for 2h), and finally placed in silicone moulds in Epon at 60°C overnight for polymerization.

### Processing using conventional techniques

Prefixed samples were incubated in 1% osmium tetroxide in PB for 2h at 4°C, before being dehydrated in increasing concentrations of ethanol at room temperature over 2.5h. Samples were then incubated in

increasing concentrations of Epon in propylene oxide before being incubated in pure Epon overnight and finally being placed in moulds in Epon at 60°C for 24h for polymerization.

#### Sectioning, imaging and quantification of EM samples

Samples were sectioned using a Leica Ultracut UCT. Semithin sections (1µm) were stained with toluidine blue to reveal myelin, and blocks were trimmed to leave only the most anterior and ventral portion of the corpus callosum. 3-5 serial ultrathin sections (70nm) were mounted on uncoated copper-palladium grids, and stained with 2% uranyl acetate (1min) and 0.2% lead citrate (4mins). Samples were imaged using a Tecnai Spirit transmission electron microscope (Thermo Fisher Scientific).

For assessment of pathology, randomly selected, non-overlapping images were taken at 6,500x magnification and the experimenter was blinded throughout the process (imaging, image analysis and quantifications). Images were analysed using the Fiji distribution of ImageJ (open source). Quantification was performed on 4-5 animals per group with at least 6 fields of view covering at least 250 µm<sup>2</sup> and at least 250 (quantification of pathologies) or 150 (g-ratios and t-ratios) myelinated axons per animal; exact numbers of features in each animal are given in Supplementary Table 1. A myelinated axon was defined as having: inner tongue vesiculation if there were multiple vesicles within the inner tongue; a split myelin sheath if there was more than one point of decompaction; myelin unfolding if the myelin sheath bulged to an extent which significantly disrupted circularity. Myelin debris was defined as multilamellar myelin sheaths lacking an axon. A myelinated axon was defined as having a degenerating axon if the axon became dark and its content of organelles very difficult to distinguish. Segmentation of the axon, the inner tongue and the myelin was carried out manually using the Fiji distribution of ImageJ. G-ratios, a measure of myelin thickness, were corrected for inner tongue diameter and calculated as:  $[\text{axon diameter}]/[\text{axon+myelin diameter}] - ([\text{axon+inner tongue diameter}] - [\text{axon diameter}])$ . T-ratios, a measure of inner tongue thickness, were calculated as:  $[\text{axon diameter}]/[\text{axon+inner tongue diameter}]$ . Diameters were calculated assuming circularity based on areas, where circularity tests were met. T-ratios are presented separately for small and large calibre axons, using a cut-off of 0.6µm as previously defined (14).

#### Immunohistochemistry

Mice were deeply anaesthetized with sodium pentobarbital (80 mg/kg) and transcardially perfused with 0.1M heparinized PB followed by 4% PFA. Brains were extracted, split into hemispheres, and post-fixed for either 1 hour (oligodendroglia) or overnight (microglia) before cryopreservation and freezing. Brains were sectioned sagittally using a cryostat at either 10µm onto glass slides (oligodendroglia) or 16µm and processed as floating sections (microglia). Sections were blocked in 10% goat serum, 0.3% triton in PBS, before being incubated with primary antibodies [Olig2 (1:200, AB9610, Millipore), APC (1:200, clone CC-1, OP80, Merck Millipore), Iba1 (1:500, 019-19741, Wako), CD68 (1:1000, clone

FA-11, MCA1957, BioRad), overnight at 4°C. Sections were washed, incubated with Alexa Fluor secondary antibodies (1:500; Life Technologies, Saint-Aubin, France) at room temperature, counterstained with DAPI, and mounted with Dako Mounting Medium.

#### Imaging and analysis of fluorescent images

Fluorescent images were acquired using a Leica SP8 confocal microscope, capturing a 10 µm (oligodendrocytes) or 12µm (microglia) thick stack with optical sections taken at 1µm intervals (objective 40x). At least 2 fields of view (290 x 290 µm) were acquired from the most anterior part of the corpus callosum, and at least 3 sections were analysed per animal. All quantifications were performed using the Fiji distribution of ImageJ and all procedures were performed with prefixed parameters. The experimenter was blinded to the genotype throughout quantifications.

The number of oligodendrocyte precursor cells and oligodendrocytes was counted manually on sections double stained for Olig2 and APC (CC-1). The number of microglial cells was counted manually on sections double stained for Iba1 and CD68. Results are expressed as the number of cells per mm<sup>2</sup>.

#### Statistics

Graphs were created and statistics calculated using GraphPad Prism 7. All data are shown as mean ± standard error of the mean (SEM). The number of biological replicates for each experiment is indicated in the appropriate figure legend. Significance was calculated using either a Student's t test or one-way or two-way ANOVA as appropriate with Tukey's or Sidak's post-hoc tests.

## **Results**

### **Optimization of the HPF/FS protocol to assess WM integrity in the corpus callosum genu from aged mice**

In the traditional HPF/FS protocol, fresh tissue is quickly dissected and frozen at high pressure without any prior chemical fixation. While this technique allows excellent ultrastructural preservation of myelin in the optic nerve, it has rarely been used on the corpus callosum (15) and, to the best of our knowledge, never on the mouse corpus callosum from a chronic disease model. The challenge is that the brain must be rapidly extracted, sectioned at <200µm, and the tissue of interest dissected and frozen in 5-10 minutes, something which, unlike the optic nerve, is extremely difficult to achieve with a tiny sample of the mouse corpus callosum. Moreover, fresh brain tissue is difficult to handle and stretching fresh tissue is suspected to cause detachment of myelin lamellae from the axon (11). Therefore, we optimized this technique to the study of the genu of the corpus callosum in mice aged from 6 to 15 months, by combining the advantages of a standard chemical fixation prior to freezing with those of

HPF and FS (Figure 1A). While a similar approach has been previously used to study brain ultrastructure in young rats, it has not been optimized for myelin preservation in older animals (16).

We found that a glutaraldehyde-paraformaldehyde fixation combining perfusion/immersion fixation preserved the ultrastructure of the WM much better than either an isolated perfusion or a sole immersion fixation (not shown). Testing different space fillers in the sample carrier revealed that PVP outperformed bovine serum albumin and yeast paste, in terms of myelin splitting. Moreover, consistent with a previous report (11), extracellular spaces seemed artefactually larger using yeast paste (Supplementary Figure 1). Finally, we noticed that thinner sections (100µm) resulted in better quality freezing, although we did not attempt to quantify this effect.

It has been suggested that myelin splitting is mainly an effect of chemical fixation and tissue dehydration. Therefore, we sought to compare qualitatively the effect of freeze-substitution with a conventional dehydration performed at room temperature, using samples of corpus callosum genu from the same prefixed specimens. The most astonishing difference was the superior preservation of myelin in the freeze-substituted samples. Indeed, myelin membranes in the freeze-substituted samples were sharper and smoother, whereas membranes in the conventionally processed samples were frequently undulating and split (Figure 1B-C). Moreover, the outer and the inner tongues — the ab and adaxonal non-myelin compartments respectively — were more visible and displayed finer details in the freeze-substituted compared to the conventionally processed samples (Figure 2).

### **Ultrastructural analysis of WM changes in the corpus callosum of CADASIL mice using HPF/FS**

The *TgNotch3*<sup>R169C</sup> mouse model (which we will refer to as CADASIL mice), is a well characterized model of CADASIL (7). Mutant mice develop WM changes in the form of increased punctate staining using a specific monoclonal antibody (SMI-94) against MBP, which is thought to mark uncompacted or degraded myelin, starting at 6 months of age and progressively worsening (8,9). These defects are more severe in the anterior and medial part of corpus callosum (6), therefore we focused our analysis on this brain region. WM samples from CADASIL and control mice were prefixed and processed in parallel using HPF/FS as described above. We assessed WM changes on electron micrographs from 4 to 5 mice per group, first at 6 months and then at 15 months of age, to examine the temporal dynamics of emerging lesions (Supplementary Table 1).

The most striking and earliest change we observed in CADASIL mice was a significant increase in the percentage of axons with myelin lamellae splitting at 6 months of age. The observation of non-compacted cytoplasmic channels within these split membranes suggests that these are true defects rather than stretching or fixation artefacts (Figure 3A-C and Figure 2 for comparison of a normal myelin sheath). This was followed at 15 months by an increase in the percentage of axons whose myelin sheath displayed vesiculation or tubulation at the inner tongue (Figure 3D-F). We also observed focal bulging of entire stacks of compacted myelin membrane, also called myelin unfolding (Figure 3G-H) and

myelin debris (Figure 3J-K), pathologies which have been described in myelin mutants or brain ageing (17,18), but in comparable numbers in CADASIL and control samples (Figure 3I, L). To further quantify changes at the level of the inner tongue, we calculated the t-ratio, a measure of the thickness of the inner tongue relative to the axon diameter (Supplementary Figure 2) (14). T-ratio measurements suggested an enlargement of the inner tongue in small calibre axons of CADASIL mice at both ages. This was further confirmed by separately analysing the t-ratio in the small ( $< 0.6\mu\text{m}$ ) versus large ( $> 0.6\mu\text{m}$ ) calibre axons (Figure 4).

Although, the percentage of myelinated axons was comparable between CADASIL and control mice at both 6 and 15 months of age (Figure 5A), the frequency distribution of myelinated axons showed that in older CADASIL animals (15 months) there were fewer large calibre myelinated axons (Figure 5B-C). To better understand any changes in myelin of CADASIL mice, we calculated the g-ratio, a measure of the thickness of the myelin sheath relative to the axon diameter, and plotted it against the axon calibre. In this analysis, we excluded the severely split fibres, as shown on Figure 3B, that might artificially increase the myelinated fibre diameter and bias the g-ratio. Moreover, due to the phenotype at the inner tongue, we used a corrected g-ratio, in which the area of the inner tongue was subtracted (Supplementary Figure 2). At both 6 and 15 months of age, the “corrected g-ratio” scatter plot showed an upshift of the cloud in CADASIL mice, suggesting myelin thinning especially in larger axons (Figure 5D-E).

Remarkably, myelin defects in CADASIL mice were not associated with overt axonal lesions at the ultrastructural level. Indeed, we found almost no degenerating axons at 6 months and a low but comparable number of degenerating axons in WT and CADASIL mice at 15 months (Supplementary Figure 3).

### **Analysis of cellular changes in the corpus callosum of CADASIL mice using immunohistochemistry**

We then sought to determine whether myelin defects observed in CADASIL mice were caused by the loss of oligodendrocytes. To achieve this, we labelled brain sections with Olig2 and CC-1 antibodies and quantified the number of oligodendrocytes and oligodendrocyte precursor cells (OPCs) (Figure 6A). To align with our ultrastructural studies, we focused our quantifications on the anterior and medial part of the corpus callosum. We selected 3 time points: before myelin pathology (4 months), and at early (6 months) and established stages of myelin defect (12 months). We found no evidence of a reduction in the number of mature oligodendrocytes (Olig2<sup>+</sup> and CC-1<sup>+</sup> cells) in CADASIL mice at any age (Figure 6B). We did, however, find an increase in the number of OPCs (Olig2<sup>+</sup> and CC-1<sup>-</sup>) at 12 months of age (Figure 6C). The fact that OPC numbers were only significantly increased in older animals, but neither at 6 nor at 4 months, suggests that this increase in OPC numbers is as a response to myelin damage.

Finally, we examined microglia cells, as these cells have been implicated in both exacerbating and repairing WM lesions. We labelled brain sections with Iba1 and CD68 antibodies and quantified the number of positive cells again in the anterior and medial part of the corpus callosum (Figure 7A). We found an increase in the number of Iba1 positive cells in older (15-month-old) but not in younger (6-month-old) CADASIL mice. However, we did not see, at any age, a significant increase in the number of Iba1 positive cells also positive for CD68, a marker of activated microglia (Figure 7B-C). These results suggest that WM changes in CADASIL mice are associated with a low-grade inflammation, which is secondary rather than being causative of them.

## **Discussion**

In this study, we took advantage of recent advances in the development of HPF/FS to improve visualization of the ultrastructure of cerebral WM and to elucidate the early myelin pathology that occurs in CADASIL, an archetypal SVD. We first optimized the protocol for the analysis of murine corpus callosum by including a prefixation step, sectioning the samples at 100µm and using PVP as a space filler in the sample carrier. Our high-resolution EM analysis of CADASIL mice shows that the pathological process affects first and foremost the myelin sheath and the inner tongue. Specifically, our ultrastructural analysis reveals that mutant mice exhibit significant splitting of myelin layers and enlargement of the inner tongue of small calibre axons from the age of 6 months. We further detect vesiculation of the inner tongue and myelin sheath thinning, especially in larger axons, at 15 months of age. Our cellular analysis suggests that these defects are not caused by a loss of oligodendrocytes, nor by a block in the differentiation of OPCs, and that they are associated at later stages with a low-grade microglial activation. Finally, our ultrastructural analysis supports the notion that myelinated axons are preserved, at least at this stage of the disease.

The use of HPF/FS has been instrumental in the elucidation of WM changes in CADASIL mice. Indeed, splitting of myelin lamellae is frequently considered as a fixation/dehydration artefact in EM samples that are conventionally processed. During the optimization of the HPF/FS procedure, we found that HPF/FS compared to the conventional approach strongly reduced splitting of myelin lamellae despite the use of prefixed specimens, which we deemed necessary. This suggests that in our hands myelin splitting is mainly caused by the room temperature dehydration steps of conventional EM sample preparation. Although we cannot formally exclude that myelin splitting might have been exacerbated in the CADASIL specimens, the observation of cytoplasm within the split area makes us confident that what we observed is a true splitting of the myelin lamellae. A second added value of the use of HPF/FS was the opportunity to better visualize pathological changes at the level of the inner tongue, which is much less visible and displays much less detail in conventionally processed samples.

In fact, we have been able to detect an abnormal vesiculation at the inner tongue and an enlarged inner tongue of small calibre axons in CADASIL mice. In a previous EM study using samples processed conventionally, we reported that myelinated axons in CADASIL mice aged 20 months displayed large intra-myelinic vacuoles containing aberrant myelin sheets usually located in the innermost layer of the myelin (8). Because it is likely that pathological changes of myelin worsen with age, we surmise that such vacuoles may correspond to the ultimate stage of a very severe vesiculation of the inner tongue. Nevertheless, we believe that the size of these vacuoles is likely exaggerated by the conventional preparation of samples. Also, using this conventional approach, the specific splitting of myelin layers, which we interpreted as an artefact, could not be appreciated in CADASIL mice. An additional strength in our current experimental design has been the use in all of our EM analyses of the same region of the corpus callosum, i.e., the medial part of the genu, that we sectioned in a way to get cross sections of transcallosal fibres. Thus, we are confident that the myelin defects we report in this study are not merely regional variations within the corpus callosum.

Our results are highly suggestive of a primary myelin injury at the early stage of CADASIL disease. In support of this interpretation is the observation that myelin defects exhibited by CADASIL mice are highly reminiscent of those recently reported in models of demyelinating diseases (15). In those models, induced either by administration of Cuprizone, anti-aquaporin 4 or anti-myelin oligodendrocyte glycoprotein antibodies into the corpus callosum, the WM exhibits a common pattern of myelin breakdown with vesiculation and enlargement of the inner tongue, and splitting of the myelin sheath. Such defects have been interpreted as a common pathological feature of degenerating myelin in diseases (15). Myelin splitting is also a common age-related myelin defect (19), however it is usually associated with focal myelin bulging and accumulation of myelin debris (18), that we found not to be significantly increased in CADASIL mice. Several elegant studies from the Simons lab suggest that this pathology (myelin splitting and vesiculation) is caused by an aberrant switching of the polymerization state of MBP molecules to a non-physiological soluble state (15,20,21).

Previously, we reported that WM damage in CADASIL mice initially manifests as punctate staining on free-floating brain sections using a specific monoclonal antibody (SMI-94) raised against human MBP residues 70-89 (8). Notably, this epitope is immediately adjacent to the two phenylalanine residues in position 90 and 91 of human MBP that are required for the polymerization of MBP (21). Moreover, the Simons lab showed that the QD9 antibody raised against human MBP residues 82-88 only recognizes MBP molecules when converted to their non-physiological soluble state and thus stains only myelin fibres undergoing myelin breakdown (15). Therefore, together these data strongly suggest that the punctate staining detected by the SMI-94 antibody in CADASIL mice corresponds to the myelin breakdown as detected in our EM analysis.

One attractive mechanism by which vessel changes associated with CADASIL could lead to a primary defect at the level of the myelin sheath is by a chronic hypoxic/ischaemic mechanism. Nawaz *et al.* have shown that phosphatidylinositol 4,5-bisphosphate (PIP2) is critically required for the stable

membrane association of MBP, and in extension for the function of MBP. Specifically they showed in acute brain slices that hydrolysis of PIP<sub>2</sub>, by increasing Ca<sup>2+</sup> entry, or altering PIP<sub>2</sub> levels by depleting the cellular ATP pool, leads to the dissociation of MBP from membranes, resulting in myelin vesiculation and breakdown (22). Calcium elevation and ATP depletion in oligodendrocytes are relevant in the context of hypoxia/ischemia (23,24). Moreover, the inner tongue, where myelin breakdown is prominent, might be especially vulnerable because it is located far away from the oligodendrocyte cell body and because of its high energy requirement (25). Yet, the reason why the enlargement of the inner tongue predominates in small calibre axons is unclear. Consistent with such a mechanism, we reported that adaptive responses of the cerebral circulation to blood pressure changes or neuronal activation were impaired early, and that resting cerebral blood flow was reduced later in CADASIL mice (7,9). Future studies are needed to record Ca<sup>2+</sup> and ATP changes in the WM of CADASIL mice to further test this hypothesis.

In conclusion, we have used high resolution EM analysis in combination with HPF/FS to study WM changes for the first time in a chronic SVD model. Our results suggest that WM lesions in CADASIL are the result of a primary myelin injury originating at the level of the myelin sheath. These defects are consistent with a hypoxia/ischemia mechanism leading to myelin splitting and vesiculation.

## Legends to Figures

### **Figure 1. Comparison between HFP/FS and conventional processing on the ultrastructure of WM corpus callosum WM.**

**A:** Schematic of the HFP/FS protocol used in this study. **B-C:** Representative electron micrographs of corpus callosum samples prepared from the left and right hemispheres of the same 15-month-old WT mouse prefixed in Karlsson-Schultz fixative, and processed either by HFP/FS (**B**) or by conventional dehydration at room temperature (**C**). Here we have selected micrographs that represent some of the frequent artefacts than can occur in old mice with the conventional processing. The sample prepared by HFP/FS displays reduced artefacts of jagged myelin sheaths and myelin sheath splitting. Scale bars= 1 $\mu$ m.

### **Figure 2. The optimized HFP/FS protocol provides finer details at the level of both compact and uncompact myelin than conventional processing.**

**A-B:** Representative electron micrographs of a myelinated axon from the corpus callosum of a 15-month-old WT mouse prefixed in Karlsson-Schultz fixative and conventionally processed (**A**) or processed by HFP/FS (**B**). **C:** Schematic of a myelinated axon in the perinodal region. **D:** Higher magnification view of the boxed regions in B showing the outer (1) and inner (2) tongues. Fine details of the myelin sheath as well as of the inner and outer tongues are better visible on the sample processed by HFP/FS. Scale bar = 200 nm (A, B) and 46 nm (D).

### **Figure 3. Qualitative and quantitative assessment of ultrastructural changes in the myelin sheath in the corpus callosum of CADASIL mice.**

Schematics (**A, D, G, J**) and representative electron micrographs (**B, E, H, K**) of the different pathological changes at the level of the myelin sheath detected in CADASIL mice: splitting (arrows in **B**) of the myelin sheath (**A,B**) with sleeves of uncompacted myelin, vesiculation at the inner tongue (**D-E**), myelin outfoldings (**G-H**), and myelin debris away from an axon (**J-K**). **C, F, I, L:** Genotype-dependent quantification of these changes in control (WT, blue dots) and CADASIL mice (*TgNotch3*<sup>R169C</sup>, orange squares) at 6 and 15 months of age: percentage of myelinated axons with a split myelin sheath (**C**), percentage of myelinated axons with vesiculation/tubulation at the inner tongue (**F**), percentage of myelinated axons with myelin outfoldings (**I**), number of myelin debris (**L**) showing in CADASIL mice significant increase in myelin splitting at both ages and significant increase in vesiculation at the inner tongue at 15 months of age. Mean  $\pm$  SEM; \*:  $P < 0.05$ , \*\*:  $P < 0.01$ ; two-way ANOVA with Tukey's post-hoc tests; n=4-5 mice per group. Scale bar = 200 nm

**Figure 4. Quantitative measurement of the inner tongue thickness in the corpus callosum of CADASIL mice**

Calculation of the t-ratio against axon diameter in small calibre (< 0.6µm) axons (A-B) and large calibre axons (> 0.6µm) axons (C-D) in WT and CADASIL mice, at 6 months (A, C) and 15 months (B, D) shows that the inner tongue is larger in small calibre axons in CADASIL mice at both ages. n=4-5 mice per group.

**Figure 5. Fewer large calibre myelinated axons with thinner myelin in the corpus callosum of CADASIL mice**

A: Percentage of axons which are myelinated in WT and CADASIL mice is comparable at both 6 and 15 months of age. B-C: Size distribution of myelinated axons with respect to the axon diameter at 6 months (B) and 15 months of age (C) shows a shift to the left in 15-month-old *TgNotch3<sup>R169C</sup>* mice, indicating fewer large calibre myelinated axons. D-E: Calculation of the corrected g-ratio against axon diameter shows that myelin is thinner (higher g-ratio) in larger axons of *TgNotch3<sup>R169C</sup>* mice at 6 months (D) and 15 months (E). n=4-5 mice per group.

**Figure 6. No loss of oligodendrocytes but an increase in the number of OPCs in the corpus callosum of aged CADASIL mice.**

A: Representative immunofluorescent images showing staining for Olig2 (green; a marker of all oligodendroglia) and CC-1 (red; a marker of oligodendrocytes) in the anterior corpus callosum of 12-month-old WT and *TgNotch3<sup>R169C</sup>* mice. White arrows mark OPCs (Olig2<sup>+</sup> CC-1<sup>-</sup>). B: Quantification of the number of oligodendrocytes (Olig2<sup>+</sup> CC-1<sup>+</sup>) at 4, 6 and 12 months of age shows no difference between WT and *TgNotch3<sup>R169C</sup>* mice. C: Quantification of the number of OPCs (Olig2<sup>+</sup> CC-1<sup>-</sup>) at 4, 6 and 12 months of age shows an increase in OPC number, but only at 12 months of age. Mean ± SEM; \*\*: *P* < 0.01; two-way ANOVA with Tukey's post-hoc tests (B, C). N= 5-8 mice per group. Scale bar = 30 µm.

**Figure 7. Increase in microglia number in the corpus callosum of aged CADASIL.**

A: Representative immunofluorescent images showing Iba1 (green; a marker of all microglia), CD68 (red; a marker of activated microglia), and DAPI (blue; nuclear marker) in the anterior corpus callosum of 15-month-old WT and *TgNotch3<sup>R169C</sup>* mice. B-C: Quantification at 6 and 15 months of the total number of microglia (Iba1<sup>+</sup>; B) and the number of activated microglia (Iba1<sup>+</sup> CD68<sup>+</sup>; C) shows a moderate increase in the total number of microglia in 15-month-old *TgNotch3<sup>R169C</sup>* mice but no difference in the number of activated microglia. Mean ± SEM; \*: *P* < 0.05; two-way ANOVA with Sidak's post-hot tests. N= 5-8 mice per group. Scale bar = 50 µm.

### **Ethics approval**

Animal (mouse) experiments were approved by our local institutional Animal Care and Use Committees (CEEA9 and CEEA34, registration numbers 95 and 19-031) and by the French government (Ministère de l'Enseignement Supérieur et de la Recherche, authorizations #03653.02 and APAFiS #21100-2019041816189580v4).

### **Author contributions**

RMR designed and performed the experiments, analysed the data and wrote the manuscript. VDD assisted with the EM and immunohistochemistry experiments. ND assisted with the data analysis and prepared the figures. GVN and XH assisted with the EM experiments and data analysis. AJ designed the study, supervised research and wrote the manuscript.

### **Acknowledgements**

We are grateful to Wiebke Möbius for technical advice on the use of HPF/FS and Ilse Hurbain for technical assistance with the HPF/FS from the cell and tissue imaging facility (PICT) of Institut Curie. Confocal images were acquired at the Institute of Psychiatry and Neuroscience of Paris (NeurImag platform); the SP8 confocal microscope was funded by a grant from Fondation Leducq. EM images were acquired at the cell and tissue imaging facility of Institut Curie or at the Imagoseine imaging core facility, member of the France BioImaging infrastructure supported by grant ANR-10-INBS-04 from the French National Research Agency. This work was supported by Fondation Leducq (Transatlantic Network of Excellence for the Study of Perivascular Spaces in Small Vessel Disease, 16 CVD 05) and the National Research Agency, France (ANR-16-RHUS-0004) to AJ.

### **Conflicts of interest**

Xavier Heiligenstein is the chief strategy officer and co-founder of CryoCapCell.

### **Data Availability Statement**

The data that support the findings of this study are available from the corresponding author upon reasonable request.

## References

1. Pantoni L. Cerebral small vessel disease: from pathogenesis and clinical characteristics to therapeutic challenges. *Lancet Neurol.* juill 2010;9(7):689-701.
2. Chabriat H, Joutel A, Tournier-Lasserre E, Boussier MG. CADASIL: yesterday, today, tomorrow. *Eur J Neurol.* août 2020;27(8):1588-95.
3. Benisty S, Reyes S, Godin O, Hervé D, Zieren N, Jouvent E, et al. White-matter lesions without lacunar infarcts in CADASIL. *J Alzheimers Dis JAD.* 2012;29(4):903-11.
4. Duering M, Zieren N, Hervé D, Jouvent E, Reyes S, Peters N, et al. Strategic role of frontal white matter tracts in vascular cognitive impairment: a voxel-based lesion-symptom mapping study in CADASIL. *Brain J Neurol.* août 2011;134(Pt 8):2366-75.
5. Schmidt R, Schmidt H, Haybaeck J, Loitfelder M, Weis S, Cavalieri M, et al. Heterogeneity in age-related white matter changes. *Acta Neuropathol (Berl).* août 2011;122(2):171-85.
6. Rajani RM, Ratelade J, Domenga-Denier V, Hase Y, Kalimo H, Kalaria RN, et al. Blood brain barrier leakage is not a consistent feature of white matter lesions in CADASIL. *Acta Neuropathol Commun.* 21 2019;7(1):187.
7. Joutel A, Monet-Lepretre M, Gosele C, Baron-Menguy C, Hammes A, Schmidt S, et al. Cerebrovascular dysfunction and microcirculation rarefaction precede white matter lesions in a mouse genetic model of cerebral ischemic small vessel disease. *J Clin Invest.* 2010;120(2):433-45.
8. Cognat E, Cleophax S, Domenga-Denier V, Joutel A. Early white matter changes in CADASIL: evidence of segmental intramyelinic oedema in a pre-clinical mouse model. *Acta Neuropathol Commun.* 2014;2:49.
9. Capone C, Cognat E, Ghezali L, Baron-Menguy C, Aubin D, Mesnard L, et al. Reducing Timp3 or vitronectin ameliorates disease manifestations in CADASIL mice. *Ann Neurol.* mars 2016;79(3):387-403.
10. Montagne A, Nikolakopoulou AM, Zhao Z, Sagare AP, Si G, Lazic D, et al. Pericyte degeneration causes white matter dysfunction in the mouse central nervous system. *Nat Med.* mars 2018;24(3):326-37.
11. Möbius W, Cooper B, Kaufmann WA, Imig C, Ruhwedel T, Snaidero N, et al. Electron microscopy of the mouse central nervous system. *Methods Cell Biol.* 2010;96:475-512.
12. Möbius W, Nave K-A, Werner HB. Electron microscopy of myelin: Structure preservation by high-pressure freezing. *Brain Res.* 15 2016;1641(Pt A):92-100.
13. Weil MT, Ruhwede T, Möbius W, Simons M. Intracerebral injections and ultrastructural analysis of high-pressure frozen brain tissue. *Curr Protoc Neurosci.* 2017;2017(January):2.27.1-2.27.18.
14. Poggi G, Boretius S, Möbius W, Moschny N, Baudewig J, Ruhwedel T, et al. Cortical network dysfunction caused by a subtle defect of myelination. *Glia.* 2016;64(11):2025-40.
15. Weil M-T, Möbius W, Winkler A, Ruhwedel T, Wrzos C, Romanelli E, et al. Loss of Myelin Basic Protein Function Triggers Myelin Breakdown in Models of Demyelinating Diseases. *Cell Rep.* 12 2016;16(2):314-22.

16. Sosinsky GE, Crum J, Jones YZ, Lanman J, Smarr B, Terada M, et al. The combination of chemical fixation procedures with high pressure freezing and freeze substitution preserves highly labile tissue ultrastructure for electron tomography applications. *J Struct Biol.* mars 2008;161(3):359-71.
17. Erwig MS, Patzig J, Steyer AM, Dibaj P, Heilmann M, Heilmann I, et al. Anillin facilitates septin assembly to prevent pathological outfoldings of central nervous system myelin. *eLife.* 23 2019;8.
18. Safaiyan S, Kannaiyan N, Snaidero N, Brioschi S, Biber K, Yona S, et al. Age-related myelin degradation burdens the clearance function of microglia during aging. *Nat Neurosci.* 2016;19(8):995-8.
19. Stadelmann C, Timmler S, Barrantes-Freer A, Simons M. Myelin in the Central Nervous System: Structure, Function, and Pathology. *Physiol Rev.* 01 2019;99(3):1381-431.
20. Bakhti M, Aggarwal S, Simons M. Myelin architecture: zippering membranes tightly together. *Cell Mol Life Sci CMLS.* avr 2014;71(7):1265-77.
21. Aggarwal S, Snaidero N, Pähler G, Frey S, Sánchez P, Zweckstetter M, et al. Myelin membrane assembly is driven by a phase transition of myelin basic proteins into a cohesive protein meshwork. *PLoS Biol.* 2013;11(6):e1001577.
22. Nawaz S, Kippert A, Saab AS, Werner HB, Lang T, Nave K-A, et al. Phosphatidylinositol 4,5-bisphosphate-dependent interaction of myelin basic protein with the plasma membrane in oligodendroglial cells and its rapid perturbation by elevated calcium. *J Neurosci Off J Soc Neurosci.* 15 avr 2009;29(15):4794-807.
23. Hamilton NB, Kolodziejczyk K, Kougioumtzidou E, Attwell D. Proton-gated Ca<sup>2+</sup>-permeable TRP channels damage myelin in conditions mimicking ischaemia. *Nature.* 28 janv 2016;529(7587):523-7.
24. Micu I, Jiang Q, Coderre E, Ridsdale A, Zhang L, Woulfe J, et al. NMDA receptors mediate calcium accumulation in myelin during chemical ischaemia. *Nature.* 23 févr 2006;439(7079):988-92.
25. Simons M, Nave K-A. Oligodendrocytes: Myelination and Axonal Support. *Cold Spring Harb Perspect Biol.* 22 juin 2015;8(1):a020479.

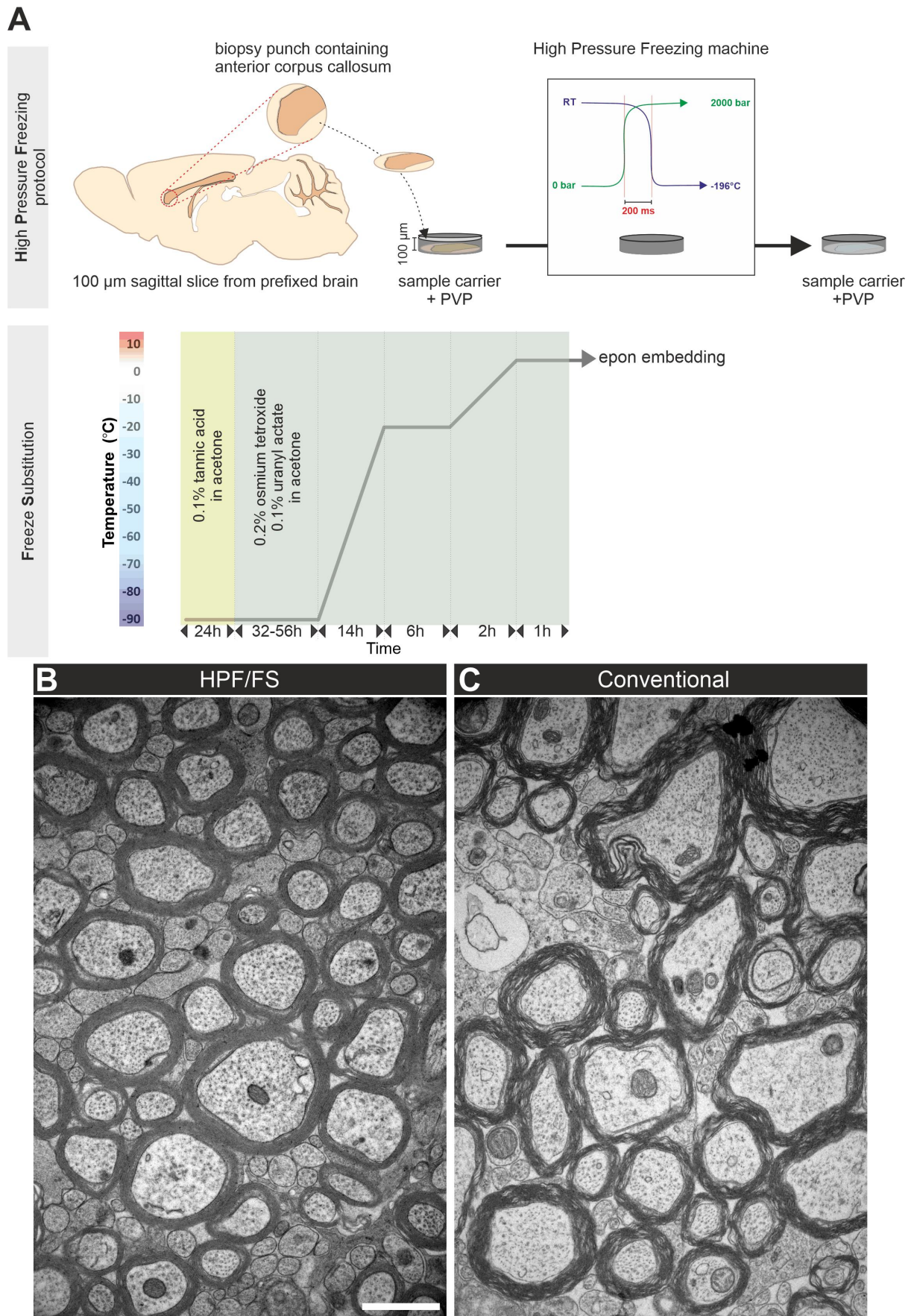


**Figure 1**

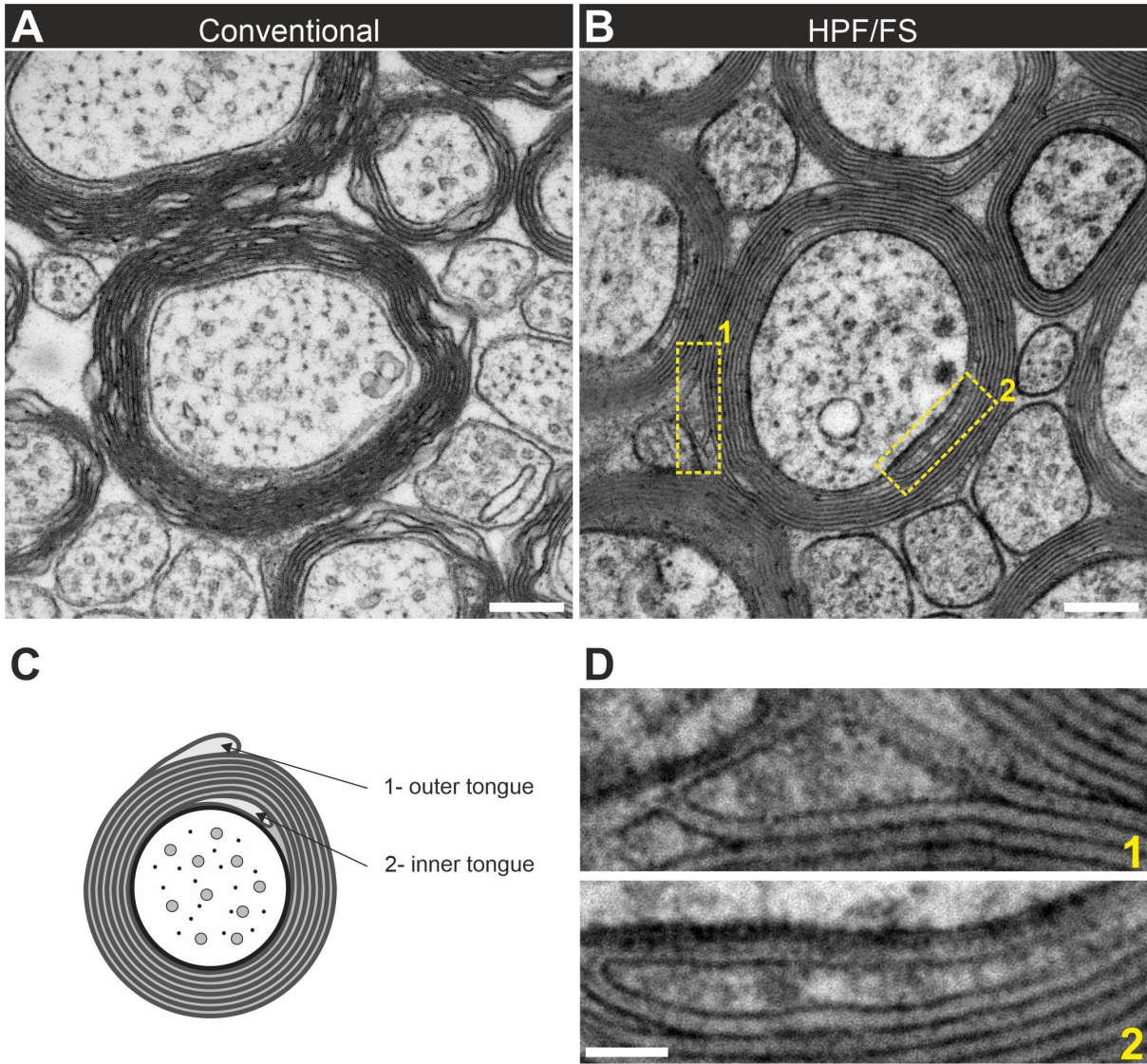


**Figure 2**

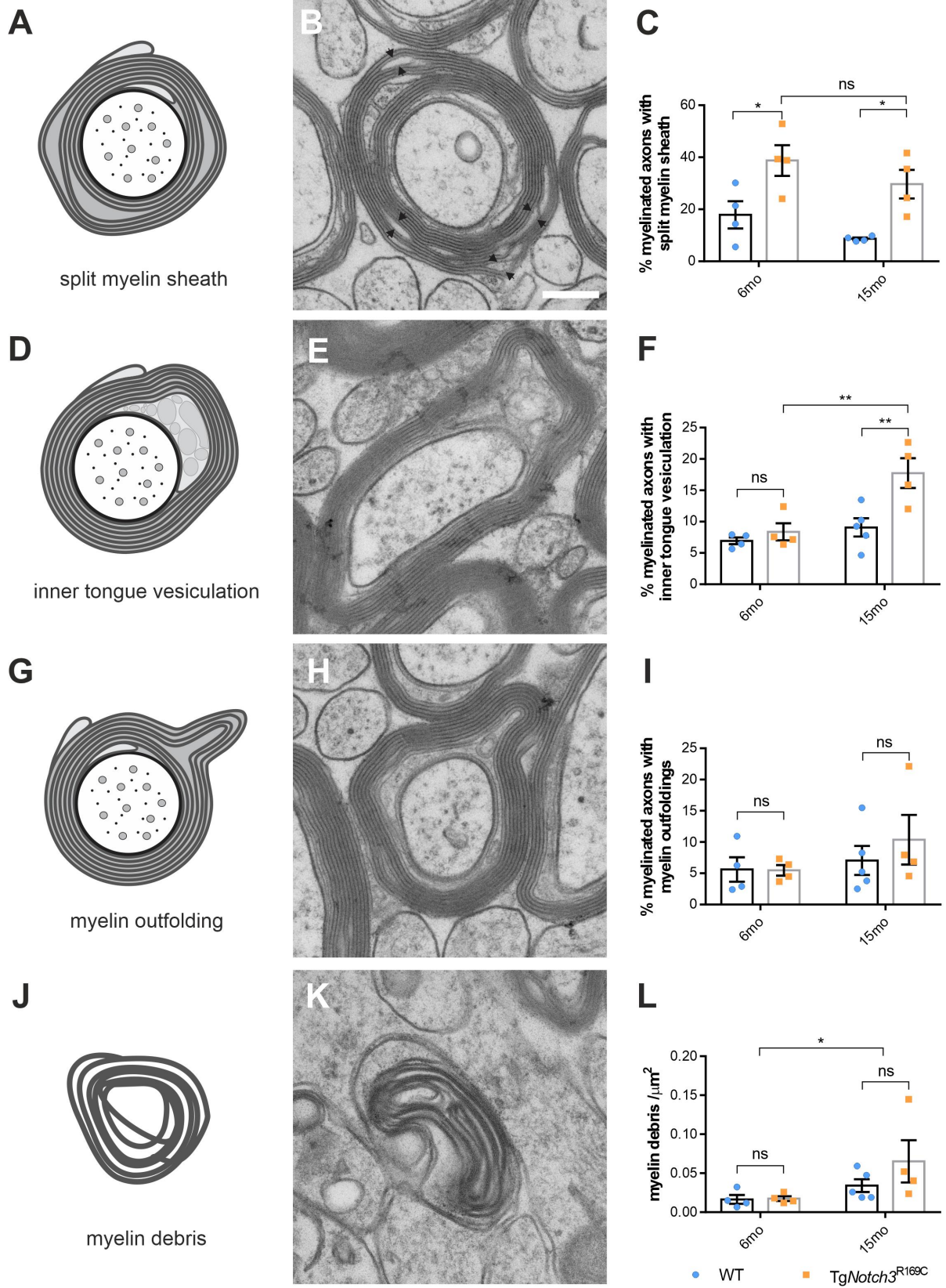


**Figure 3**

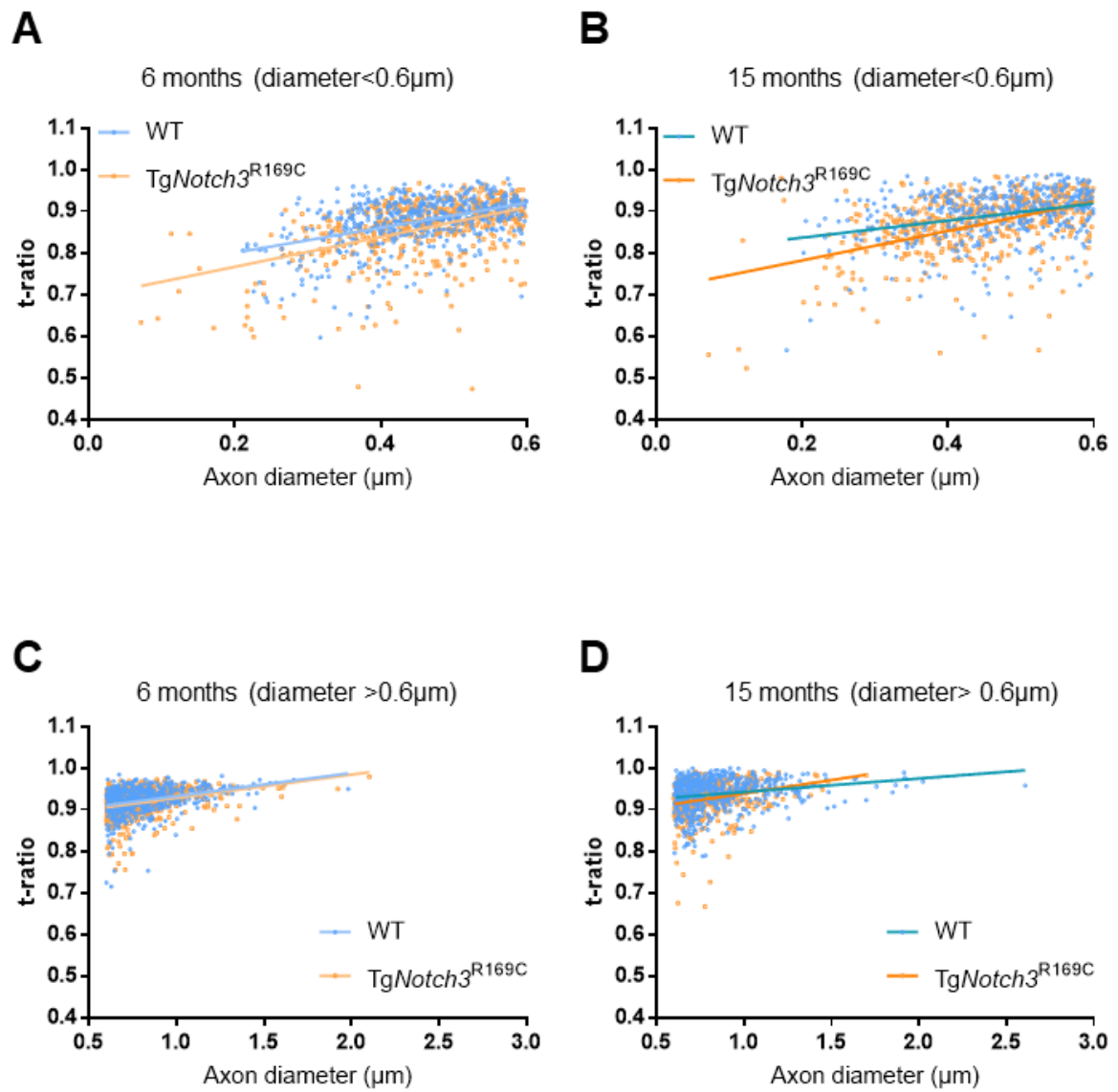


**Figure 4**

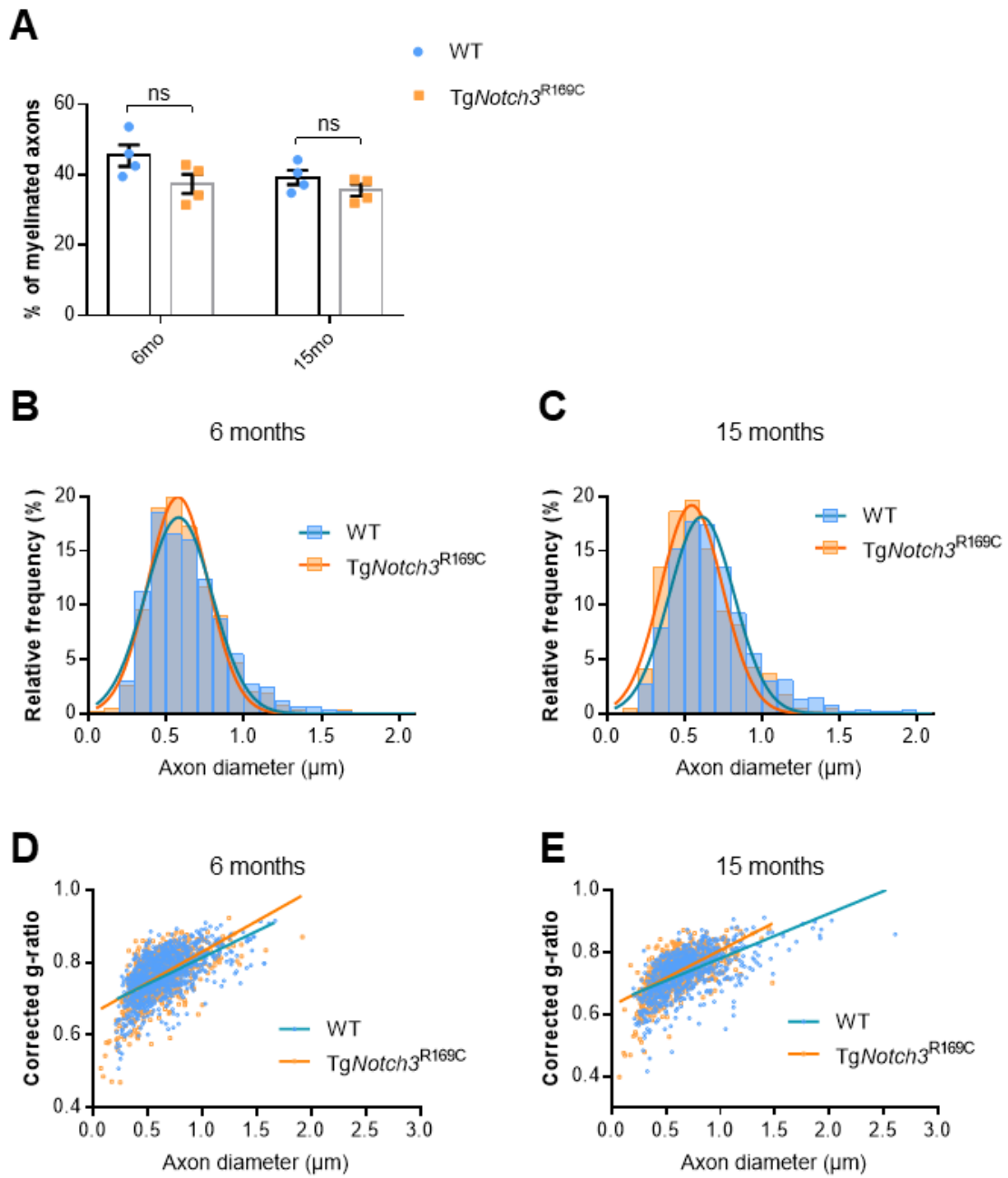


**Figure 5**

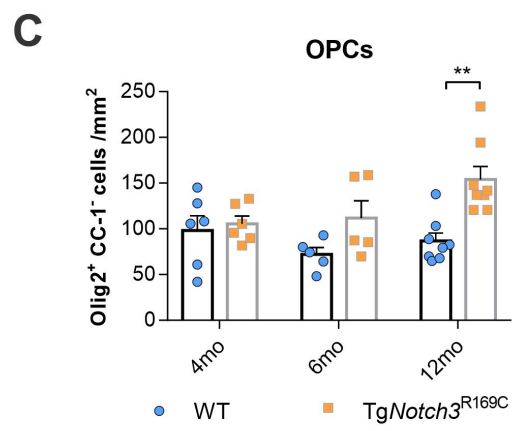
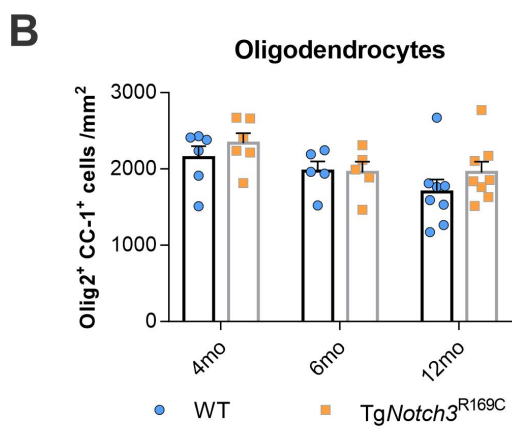
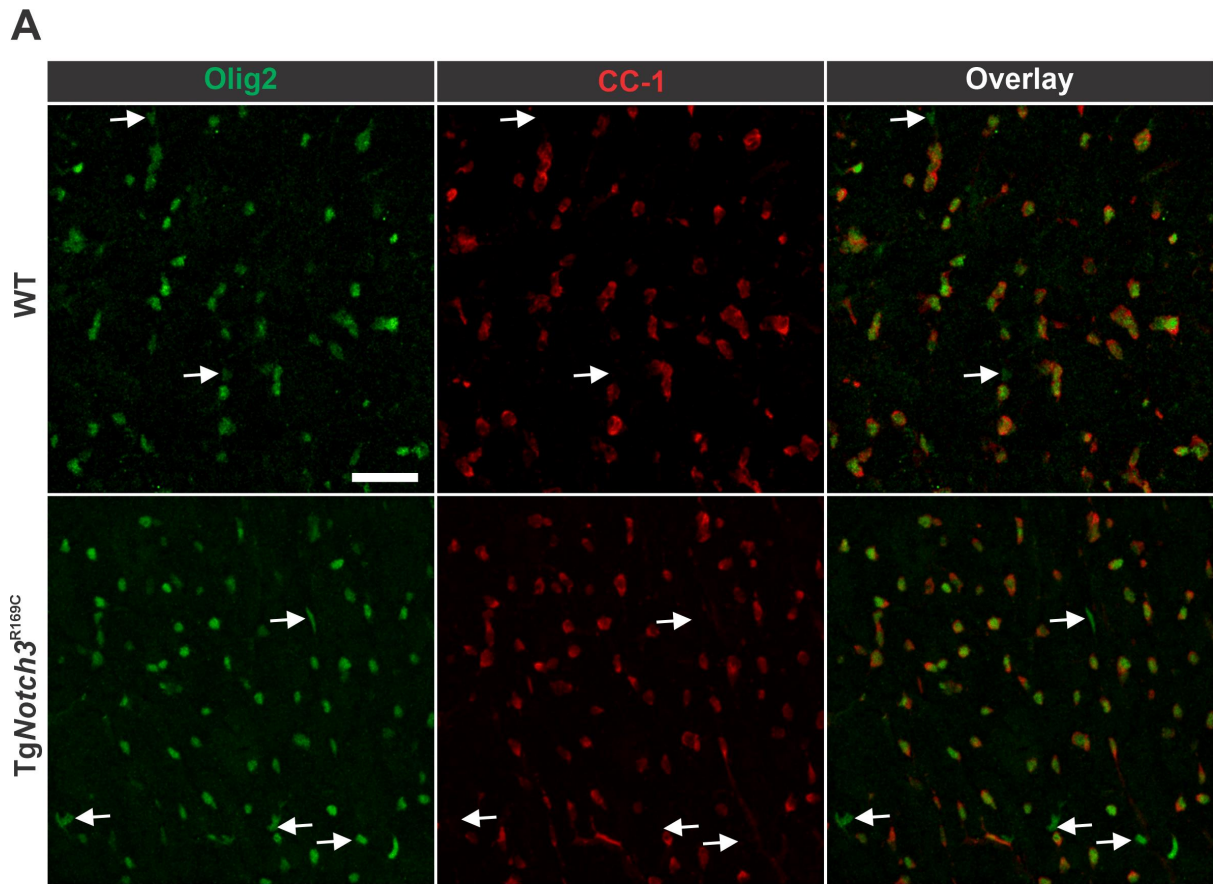


**Figure 6**

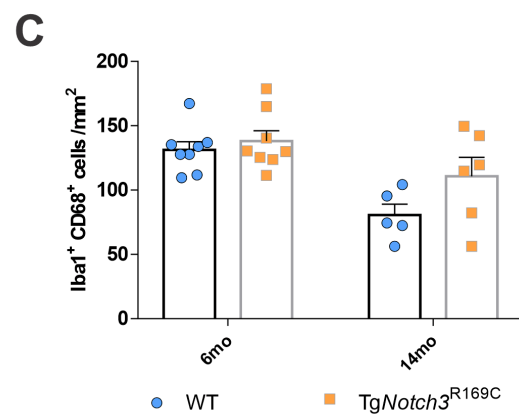
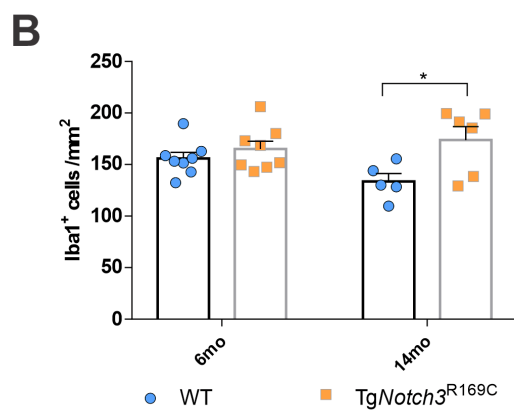
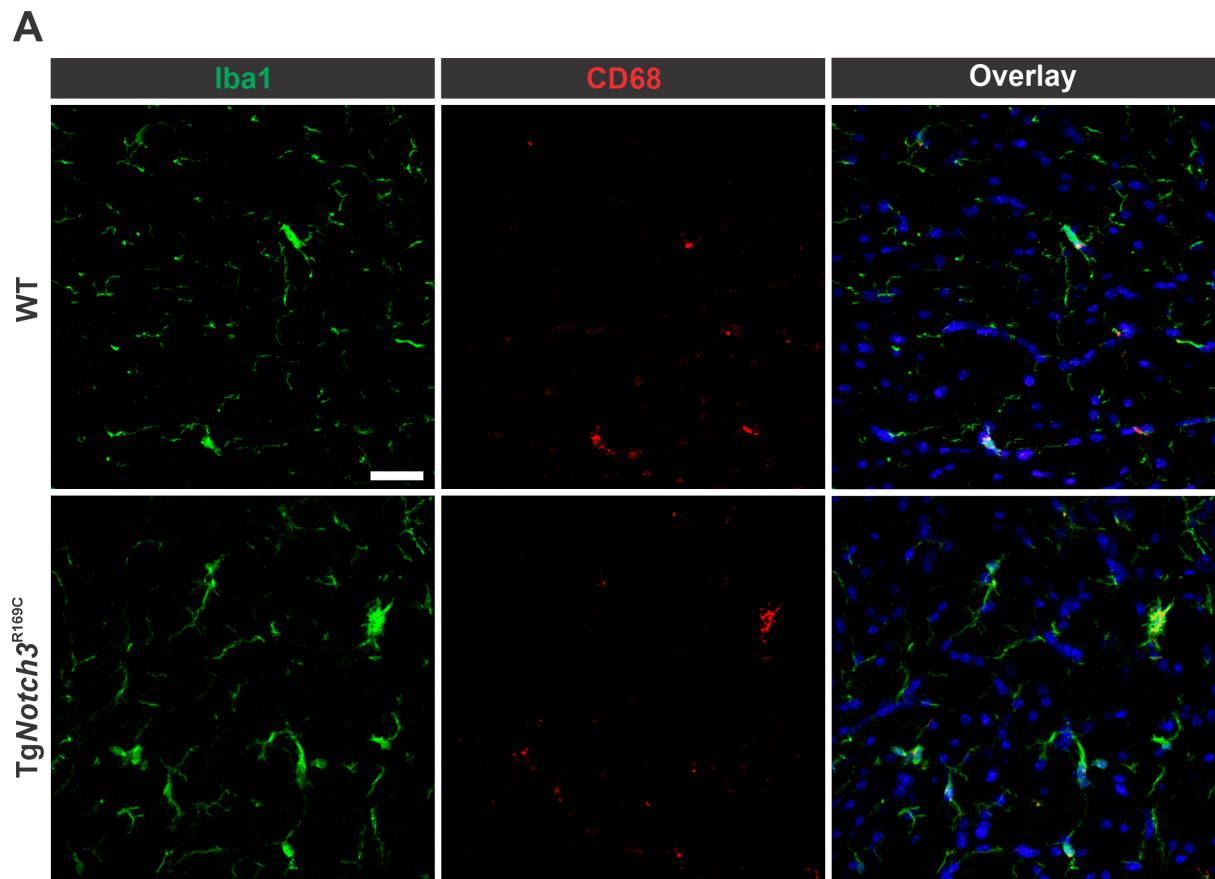


**Figure 7**